Nanoscale

COMMUNICATION

View Article Online
View Journal | View Issue

Cite this: *Nanoscale*, 2025, **17**, 12087

Received 16th January 2025,
Accepted 13th April 2025

DOI: 10.1039/d5nr00229j

rsc.li/nanoscale

Evidence of Au(111) topological states in a kagome analogue lattice and their robustness beyond ultra-low temperatures and defect-free conditions†

Dave Austin,[a] Ana Barragán,[b,d] Eric D. Switzer,[a] Sara Lois,[b] Ane Sarasola,[b,e] Duy Le,*[a] Talat S. Rahman[a] and Lucia Vitali*[b,c,d,f]

The experimental realization of kagome lattices that exhibit the predicted coexistence of topological states with high electron kinetics and non-dispersing quantum states remains challenging. Additionally, the robustness of these states against structural perturbations has rarely been explored. Here, we report on the formation of an analogue kagome structure *via* the electrostatic self-assembly of 4,7-dibromobenzo[*c*]-1,2,5-thiadiazole (2Br-BTD) molecules on Au(111). Local spectroscopic measurements, supported by theoretical calculations, reveal that the weak molecular coupling reshapes the topological-induced Shockley surface state of Au(111) by imposing a (7 × 7) periodicity, resulting in new band crossings. The molecular overlayer favours the opening of electron gaps at these positions manifested as sharp peaks in d*I*/d*V* spectra and electron localization in either the hexagonal or triangular sublattices of the kagome structure. To explore the robustness of these topological states, we monitored their stability under varied conditions, including different temperatures, the unaltered herringbone reconstruction of the Au(111) surface and local structural relaxation of the molecular assembly. These results demonstrate the degree of topological protection of these states, which holds potential for fundamental and applied research.

[a]*Department of Physics, University of Central Florida, 4000 Central Florida Blvd., Orlando, Florida 32816, USA. E-mail: duy.le@ucf.edu*
[b]*Donostia International Physics Center (DIPC), Paseo M. Lardizabal 4, 20018 San Sebastián, Spain*
[c]*Advanced Polymers and Materials: Physics, Chemistry and Technology, Chemistry Faculty, University of Basque Country (UPV/EHU), Paseo M. Lardizabal 3, 20018 San Sebastián, Spain*
[d]*Centro de Física de Materiales CFM/MPC (UPV/EHU), Paseo M. Lardizabal 5, 20018 San Sebastián, Spain. E-mail: lucia.vitali@ehu.es*
[e]*Departamento de Física Aplicada, University of Basque Country (UPV/EHU), E-20018 San Sebastián, Spain*
[f]*Ikerbasque Research Foundation for Science, Plaza Euskadi, 5, Bilbao 48009, Spain*

†Electronic supplementary information (ESI) available: Experimental and computational methods; comparison of PDOS of kagome lattice in the free-standing and Au(111) supported structures; PDOS of Au(111) surface: PDOS of (1 × 1) surface/band structure of Au(111) in (7 × 7) surface supercell; local surface potential variation; structure and strain relaxation. See DOI: https://doi.org/10.1039/d5nr00229j

Recent research has explored various strategies to engineer topological states in different band structures, including both massless and massive linearly dispersive systems. Theoretical predictions have unveiled the potential coexistence of perfectly flat bands with Dirac cone dispersions in systems structured in moiré, Lieb, and kagome lattices. These lattices, which foster contrasting effects like high electron localization and ultra-fast transport, serve as platforms for studying unconventional phenomena such as superconductivity, magnetism, or intriguing effects such as electron correlation and exciton condensation.[1–4] Despite these desirable electronic properties, the experimental realization of such crystal structures has lagged due to challenges in identifying the ideal solid-state system. Furthermore, there remain uncertainties regarding their robustness against lattice perturbations, as this aspect has not been thoroughly investigated.

Elegant approaches, exemplified by low-temperature manipulation of individual CO molecules on supporting substrates[5–8] or by photonic systems,[9–11] have led to the engineering of electronic states through tailored electron confinement and light interference. These analogue systems emulate molecular structures, enabling the investigation of exotic states of matter in a controlled manner. However, realizing the full potential of these engineered topological states in quantum information, technology, and optoelectronics requires the scalability of the host system and its stability at room temperature. Alternative solid-state approaches based on coordination chemistry and on-surface chemical synthesis, like in metal–organic or polymeric networks[12–20] and exfoliated inorganic 2D systems, have been extensively investigated.[1–4] Nonetheless, clear evidence of the combined presence of topological states in self-assembled structures, such as in the kagome lattice and their robustness remains limited. Here, we characterized topological states in an analogue kagome lattice formed by a purely organic layer of weakly-interacting 4,7-dibromobenzo[*c*]-1,2,5-thiadiazole (2Br-BTD) molecules on the Au(111) surface. *Ab initio* calculations confirm that, despite the weak coupling, the 2Br-BTD mole-

cules modify the topologically-derived Shockley surface states of Au(111)[21] through the sulfur termination. The surface potential is locally modified and the surface band is reshaped, resulting in two Dirac cones crossed by less dispersive bands. The molecular layer induces the opening of electron gaps and the formation of saddle points reminiscent of flat band structures. This leads to electron localization, an effect observed by scanning tunneling microscopy and spectroscopy at low temperatures and confirmed by first-principles simulations. The robustness of the two topological states against temperature variations and structural perturbation of the crystal lattice is accessed by exploiting the persistence of the herringbone reconstruction and local structural relaxation of the molecular lattice. This characterization constitutes a significant finding of this work. These investigations suggest different degrees of robustness of two topologically non-trivial states.

Fig. 1 displays representative STM topographic images of the Au(111) surface after the adsorption and self-assembly of the 2Br-BTD molecules. These images, combined with the structure modeled using density functional theory (DFT) (see methods in ESI SI1†) illustrate the formation of a characteristic kagome lattice. Fig. 1a shows six triangles surrounding a central hexagon. In contrast, Fig. 1b and c, imaged at lower voltage, reveal the molecular assembly on the same surface position. The considerable differences between these topographic images make it challenging to correlate the corresponding contrast observed in Fig. 1a with the corresponding molecular assembly. Triangles and hexagons sketched in the images guide the eye through the intricate molecular network, facilitating the comparison between images with a noticeable bias-dependent contrast. Based on the molecular appearance, we proposed a model (Fig. 1e) in which the six molecules at the center of the hexagons spin around a pore delimited by one of their Br atoms, thus forming a Br_6 nodal structure. Each of these molecules interacts with two nearby molecules at the other halogen termination, collectively forming Br_3 nodal positions at the center of each triangle (see ESI SI2†). The vertices of the triangles point towards the thiadiazole groups of the neighboring molecules. These chiral Br_3 and Br_6 synthons alternate in space in a purely organic structure, defining the two sublattices of a chiral kagome pattern. Consequent simulated STM images shown in Fig. 1d and f are in agreement with experimental STM images shown in Fig. 1a and c, respectively, validating our proposed model. The kagome structure observed here differs from previously reported systems[14,16,17,19,20] in two key aspects: (i) the 2Br-BTD assembly forms an open-shell structure, in which the kagome pattern is not geometrically delimited by the molecules and coordinating atoms, unlike the previously reported metal–organic assemblies forming an Archimedean tiling structure.[14,23] (ii) The 2Br-BTD network is controlled by weak electrostatic molecular interactions.[22] The cohesion of this molecular assembly, predicted for a free-standing system, stems from a series of synergistic secondary van der Waals bonding.[22] This structure is only minimally modified by the molecular interaction with the Au(111) surface except for a small molecular tilt. DFT calculations (Fig. 1e) show that the adsorbed molecules are nearly parallel to the surface, with the molecular Br functional groups positioned slightly closer to the surface.

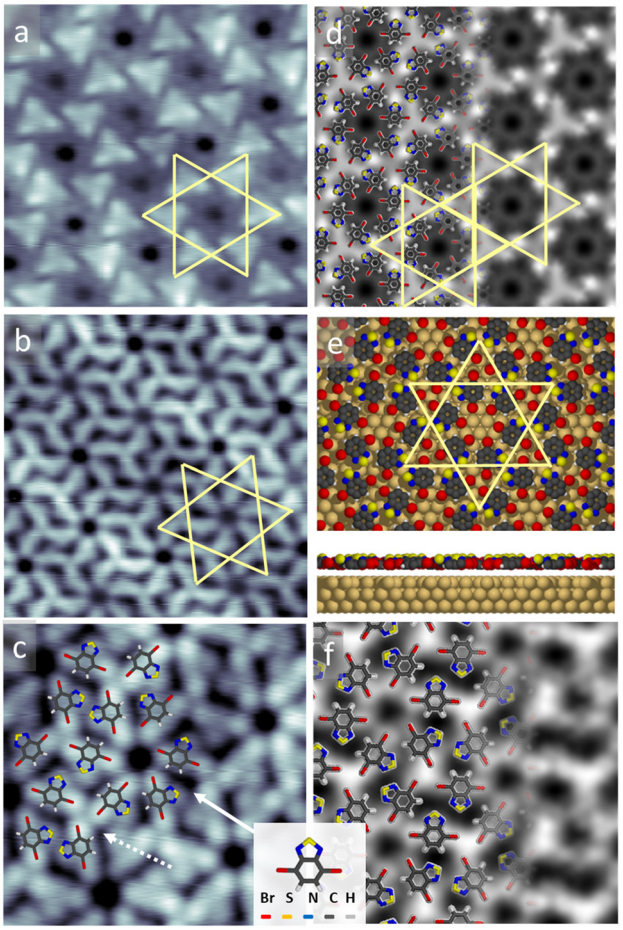

Fig. 1 Topographic images and modeling of the 2Br-BTD self-assembled network' structure on the Au(111) surface. (a and b) Constant current topographic images of the 2Br-BTD network (a) 1.80 V, 0.2 nA; (b) 0.85 V, 0.4 nA (image size: 8 nm × 8 nm). (c) Higher resolution topographic image (−0.05 V, 1 nA; 4.5 nm × 4.5 nm) with a superimposed sketch of the molecular structure. Arrows highlight the Br_6 and Br_3 nodal interactions (d) Simulated STM images with a bias voltage of 1.5 V. Note that because energy levels predicted by DFT are not the same as determined in experiment, there is a slight difference in the bias voltage used in simulated STM image (Fig. 1d) and that used in experiment (Fig. 1a). (e) Model of the 2Br-BTD on Au(111) system used for DFT simulations. (f) Simulated STM image with a bias voltage of −0.05 V. Sketched triangles and the hexagon guide the eyes to the molecular assembly that generates the electronic kagome appearance.

Differential conductance dI/dV spectra collected at the positions indicated by dots in the topographic image (inset) are shown in Fig. 2. The increased density of states observed at −1.0 V and 1.8 V in the occupied and unoccupied energy regions (black arrows), respectively, correspond to the highest occupied molecular orbital (HOMO) and lowest unoccupied molecular orbital (LUMO) states of the adsorbed 2Br-BTD molecules, confirming the semiconducting character of the

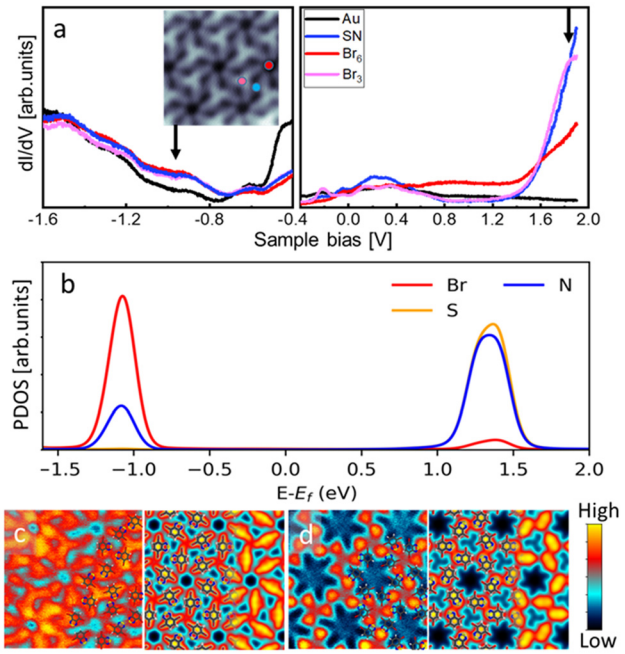

Fig. 2 Local spectroscopic characterization. (a) d*I*/d*V* spectra at selected positions as shown in the topographic image in the inset. (b) Calculated LDOS structure. (c and d) Experimental differential conductance maps (left panels; red colour being the more intense) at c.: −1.0 V, 0.4 nA; d.: 1.8 V, 0.1 nA and corresponding simulations (right panel, −1.1 V and 1.4 V, respectively) (image size 4.5 × 4.5 nm).

overlayer. These observations align with DFT calculations predicting two peaks at −1.1 eV and 1.4 eV, respectively (Fig. 2b). The excellent agreement between theoretical and experimental results is evident when comparing the spatial distribution of the d*I*/d*V* signal in constant energy maps with the conductance maps calculated by DFT at these energies (Fig. 2c and d). Note here that we used a slightly smaller voltage in simulating STM image because of the known limitations of DFT in predicting unoccupied states. This comparison supports the conclusions that the frontier orbitals are dominated by Br and N atoms for the occupied states and by states localized at S–N and Br atoms for the unoccupied states. Altogether, the electronic properties of the 2Br-BTD molecules on Au(111) are similar to those predicted for the gas phase system[22] (ESI SI3†), indicating a weak molecule–substrate interaction and negligible charge transfer (ESI SI4†).

Having identified the HOMO and LUMO molecular structures, the energy range enclosed between these two frontier orbitals should reflect solely the electronic properties of the Au (111) surface yet it reveals a richer physics. The low energy features observable in the low energy range in Fig. 2 are better seen in the series of d*I*/d*V* spectra measured along the white line traced in the topographic image (Fig. 3a) and presented as a colour scale (Fig. 3b). As the probed positions move along the line across three molecular supercells towards the Au(111) surface on the image's right side, the spectra reveal an electronic structure that can neither be attributed to the orbitals of the 2Br-BTD molecules, since the probed energies fall within the HOMO–LUMO gap (Fig. 2), nor to the ones expected for the Au(111) structure.

Specifically, the Au(111) surface state remains visible beneath the molecular structure, albeit its onset shifts upward from −440 mV on the bare Au(111) surface (right side of the Fig. 3b) to −260 mV, on average, on the molecular superstructure (Fig. 3b and c). This shift, along with the persistence of the surface state, indicates a weak interaction between the assembled molecules and the Au(111) surface, akin to the effect of noble gas adsorption on metal surfaces and assigned to Pauli repulsion of electrons.[24,25]

Additionally, Fig. 3b reveals intriguing periodic modulations of the electronic properties of the system around the Fermi level in the probed molecular region. The d*I*/d*V* spectra selected at the Br_3 and Br_6 nodal positions and shown in Fig. 3c reveal two sharp resonant states at 130 mV and 850 mV, respectively. The pronounced sharpness of these states suggests significant electron localization and it is considered a preliminary condition for electron correlation.[15,26] To explore the nature of these electronic features, we have calculated, using DFT, the band structure of the system projecting on the p_z orbital of the Au atoms of the Au(111) surface, considering the (7 × 7) periodicity constrained by the monolayer of 2Br-BTD. The p_z orbital of the surface Au atoms is chosen because it is shown to be the main component of surface states of the Au(111) surface (see ESI Fig. 5.3 and 5.4†). These calculations reveal multiple bands crossing at different points along the ΓKM high symmetry direction of the surface Brillouin zone (Fig. 3d). Interestingly, a similar band structure can also be obtained for the clean Au(111) system, considering the same (7 × 7) geometry (ESI SI5†). This observation outlines that the topologically derived Shockley surface states band of Au(111)[21] undergoes a deep reshaping. The main features are only marginally, though notably, modified by the adsorption of the 2Br-BTD molecules. Specifically, the surface states of Au(111) retain the parabolic dispersion visible at the lowest energy, although they are slightly depleted and shifted towards higher energy upon the molecular assembly, consistent with experimental observations. Moreover, notable features emerge from these calculations at the band crossing at the Γ and K points of the Brillouin zone at energies of approximately 200 mV and 900 mV, both in the clean Au(111) surface and in the 2Br-BTD/Au(111) systems. At these energies, we observe two pairs of Dirac cones and additional bands exhibiting flatness or saddle points. In the molecular system, gaps of the order of 4.4–39.14 mV open between the Dirac cones (Fig. 3e and f, respectively), lifting the degeneracy observed in the (7 × 7) cell of the clean Au(111) surface. Despite minor changes, the other band observed at these energies preserve the short flat segment (Fig. 3e and f), aligning with the experimentally observed sharp resonances at 130 mV and 850 mV. However, the computed local density of states at the center of Br_3 and Br_6 regions reproduces the sharp peaks at these energy levels (see Fig. SI6.1†).

The gapped Dirac cones and non-dispersing flat bands in momentum space are important features that characterize

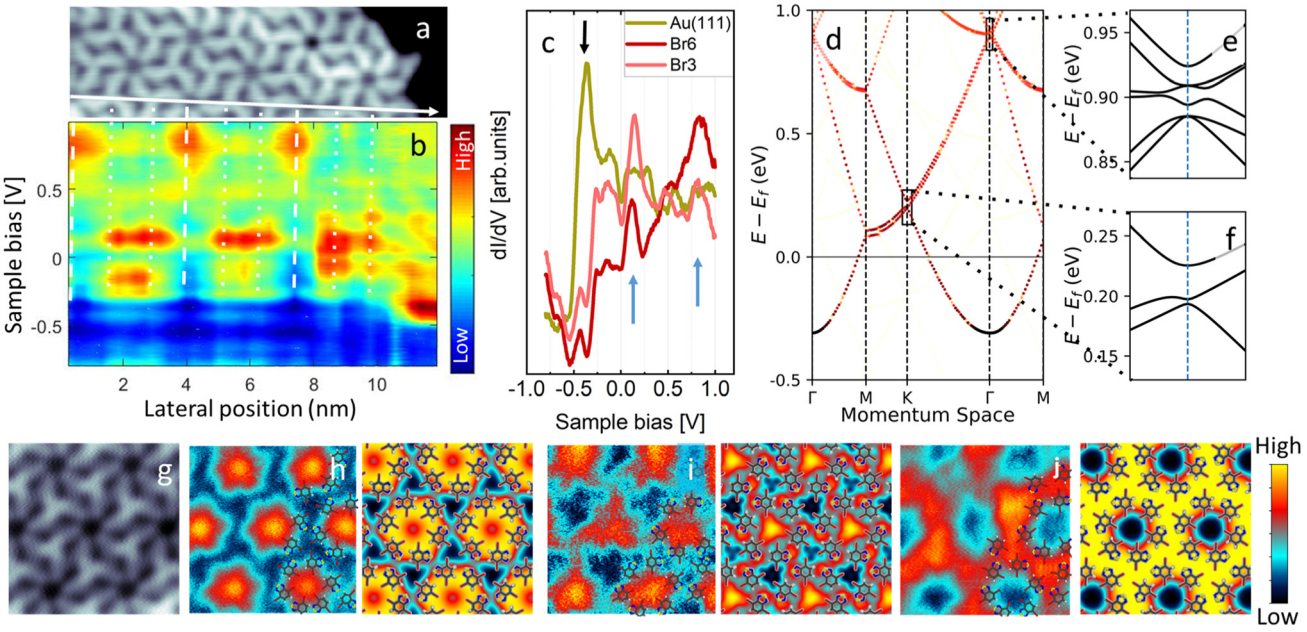

Fig. 3 Electronic properties of the 2Br-DBT kagome structure on Au(111) in the region near the Fermi level. (a) Topographic image (image size: 12 nm × 3.8 nm). (b) Colour scale representation of a series of d*I*/d*V* spectra measured along the arrow in panel *a* within the energy gap of the semiconducting layer. Dashed and dotted lines highlight the position of Br_6 and Br_3 nodal configurations, respectively. (c) Selected d*I*/d*V* spectra. The black and blue arrows point to the onset of the Au(111) surface state and the sharp resonant states, respectively. (d) Calculated (DFT) contribution of Au surface atoms' p_z orbital to the band structure along the high symmetry path ΓMKΓM. (e and f) Details of the band structure at the two topological states. (g) Topographic image (4.5 nm × 4.5 nm). (h–j) Experimental differential conductance maps for the states observed near the Fermi level (850 mV, 0.3 nA; 500 mV, 0.1 nA; and 150 mV, 0.1 nA) (left panels) and their corresponding simulated images by DFT (right panels). The red (blue) colour indicates the higher (lowest) signal intensity.

topological non-trivial states of kagome lattices. In our DFT calculations, the degree of flatness observed falls short of the ideal perfection theoretically expected for such systems and is rarely observed experimentally in inorganic structures.[1–5] However, analogue systems have recently shown that the degree of band flatness depends on the distance between electron scattering centers and increases with the increasing strength of their interacting potential.[28] A better agreement has been captured by our tight-binding model for the diatomic Kagome lattice (see ESI Fig. 7†), which further supports the topological nature of these confined states in the hexagonal and triangular sublattices of the kagome architecture.[1,27,28]

The electron localization at the hexagonal (Br_6 positions, Fig. 3h) and the triangular site (Br_3 positions, Fig. 3j) is observed at the energies corresponding to the gapped band crossing *i.e.* to the sharp peaks in Fig. 3b and c. This indicates that the individual S atoms confine at least partially the surface electrons in the two Br nodal positions, a behaviour expected for topologically non-trivial bands in kagome lattices.

In contrast, the intermediate energy state observed experimentally at 500 mV and associated with a calculated parabolic dispersing band around 650 mV at momentum M, shows mixed contributions showing the density of states at each second Br_3 position (blue and light blue areas in Fig. 3i) as well as at the Br_6 sites. This condition is expected for a non-negligible hopping integral, *i.e.* for a not confined states. This spatial distribution confirms the trivial nature of this state, as opposed to the expected true localization of the non-trivial states discussed above.

It is worth underlining that the emergence of the topological states in this system is not of a molecular origin, as often observed in coordination and metal–organic networks.[12–18] It also does not reflect a simple folding of the Au(111) surface states induced by the molecular overlayer. Molecular adsorption and its ordered assembly are fundamental to the engineering of this topological non-trivial state through gap opening at the band crossing. Previous studies have demonstrated that accurate manipulation of individual CO molecules at 4 K on copper surfaces can induce high electron localization and correlation and ultra-fast electron mobility in massive flat bands or massless Dirac states. In our case, the Au(111) surface state is spontaneously reshaped into an analogue kagome system[5–8,28] by mutual electron interference caused by the molecular assembly at room temperature. The effect of this assembly goes beyond imposing a new periodicity to Au(111) and it is fundamental to open gaps at the new band crossings, which is fundamental for the non-triviality of the topological state (Fig. 3e and f). The minor degree of molecular hybridization (see ESI SI.3†), along with the variation of the local potential at the sulfur atoms of adjacent 2Br-BTD molecules (see ESI SI.8†), suggests that the two chalcogen atoms induce electron localization to the Br_3 and Br_6 regions, triggering the

formation of this analogue lattice visible in topographic and energy-resolved imaging. At the Br_6 and Br_3 positions, notwithstanding the limited extension in the reciprocal space of the flat band structure[1,22,28–31] and the weak S–Au interaction, electron localization is observed in the two network sublattices (Fig. 3b).

The importance of this evidence of topological states would be diminished without demonstrating their invariance against perturbation of the crystal order and their persistence at higher temperatures, which are assessed in the present work. First, we considered the primary source of disorder that stems from the unaltered and persistent herringbone reconstruction beneath the molecular network. This reconstruction inherently disrupts the long-range crystal order of the system, however, neither our theoretical simulations nor the one of Yan *et al.*[21] for their model system accounts for it. Despite this, the striking similarity between our experiment and theoretically predicted images seen in Fig. 3 suggests that the topological states remain stable. Furthermore, our energy-resolved images over a large area of the surface, which include various segments of the herringbone reconstruction, provide additional evidence that the topological states at 0.13 V and 0.85 V are unaffected by this reconstruction (Fig. 4a–c). Remarkably, while the low energy state is consistently observed in all triangles of the kagome lattice, the higher energy state exhibits selective attenuation at well-defined positions, though it remains visible. Comparing these attenuated sites with the topographic image it becomes clear that these positions can be associated with the few Br_6 nodal centers visualized as darker pores in Fig. 4a. In these sites, the intermolecular distance between neighbouring Br terminations is increased (see also ESI SI2†), likely facilitated by their non-bonding configuration,[22] whose modification does not affect the energy of the system. Although these larger-distance positions are more frequently close to the herringbone lines, as evidenced by the dashed lines in Fig. 4c, the structural relaxation does not occur consistently in all Br_6 nodal sites (see arrows in Fig. 4a) situated in the proximity of the Au(111) reconstruction. Thus, we conclude that the signal attenuation is due to structural relaxation at the molecular layer. It is worth noticing that this crystal lattice perturbation does not modify the state at 130 mV. Additionally, we explored the robustness of the states by increasing the temperature of the system up to 77 K (Fig. 4d–f). Compared with the constant-energy images of Fig. 4b and c (measured at 4 K), these topological states appear modified, especially at the lowest energy. However, they remain visible. Consequently, both topological states have a non-trivial nature, although they show a different degree of protection against structural defects and temperature variation. We speculatively assign such behaviour to the size and strength of the gap opened at the corresponding band crossing in analogy to the observations of Pan *et al.*[2]

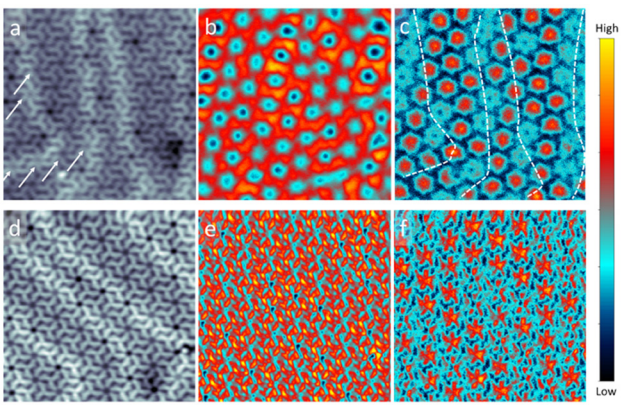

Fig. 4 Robustness of topological states against structural disorder and raising temperature (a) topographic image (a. 0.85 V, 0.3 nA) and differential conductance maps (b) 0.13 V, 0.3 nA and (c) 0.85 V, 0.3 nA measured at 4 K. The measured area crosses different sites of the herringbone reconstruction of Au(111), including relaxed configurations of the Br_6 assembly of the 2Br-BTD molecules, which appear darker in the topographic image. The arrows in panel a highlight a few of the Br_6 assemblies on top of the herringbone lines that do not undergo structural relaxation. Dashed lines in (c) indicate the position of the herringbone reconstruction observed in the topographic image. (d) Topographic image (a. 0.85 V, 0.2 nA) and differential conductance maps at (e) 0.13 V, 0.2 nA and (f) 0.85 V, 0.2 nA measured at 77 K (image size 15 nm × 15 nm).

In conclusion, we have described the formation of an analogue kagome lattice, providing evidence of the topologically non-trivial states formed at the gapped band crossing of a 7 × 7 folded Au(111) surface state. This electron-driven structure is observed in a purely organic self-assembled structure of 2Br-BTD molecules on the Au(111) surface. The molecular self-assembly introduces a new periodicity in the system, which significantly modifies the band structure of Au(111) where the formation of Dirac cones is observed. The presence of the 2Br-BTD molecules is fundamental for the gap openings and hosting of weakly dispersive states at 130 mV and 850 mV, respectively. These states localize charge carriers in the triangular sublattice of the kagome architecture as confirmed by scanning tunneling spectroscopy and density functional theory calculations. The topological protection and the robustness of these states have been assessed against two principal crystal-lattice perturbations: the herringbone reconstruction of the Au(111) surface and the local relaxation of the molecular structure. Our findings show that these states remain stable under such perturbations despite an attenuation of the highest energy state. The topological protection is retained even when the system is subjected to temperature variations of up to 77 K, although some modifications are observed, especially at the lowest energy. The mechanism controlling the different degrees of robustness is still unclear.

Finally, the chiral character observed in this structure at Br_3 and Br_6 positions breaks the mirror symmetry in the topological images and electronic structure calculations (ESI 2†). Overall, this work not only confirms the viability of using molecules to engineer topologically protected states but also provides valuable insights into their stability towards more realistic conditions, laying a foundation for future potential applications in advanced quantum technologies. The inter-

play between chirality and topologically protected states offers promising avenues for future research, particularly in the development of electronic and optical switching devices.[32–34]

Data availability

All data that support the findings of this study are included within the article (and any ESI files†). Data presented in all Figures are available at the Zenodo repository (**https://doi.org/10.5281/zenodo.15190434**).

Conflicts of interest

There are no conflicts to declare.

Acknowledgements

LV acknowledges the funding of the Basque Government (Grupo Consolidado IT1453-22 and PIBA_2024_1_0011), of the European Union NextGenerationEU/PRTR-C17.I1, and the IKUR Strategy under the collaboration agreement between the Ikerbasque Foundation and MPC on behalf of the Department of Education of the Basque Government. TSR, DL and EDS acknowledge funding from the US Department of Energy under grant DE-FG02-07ER46354 that supported the theoretical effort presented here. DA acknowledges the support of the National Science Foundation under grant CHE-1955343. SL acknowledges funding from the Spanish State Research Agency project PID2019-107338RB-C66. Computational resources were provided by the National Energy Research Scientific Computing Center (NERSC).

References

1 M. Kang, S. Fang, L. Ye, H. C. Po, J. Denlinger, C. Jozwiak, A. Bostwick, E. Rotenberg, E. Kaxiras, J. G. Checkelsky and R. Comin, *Nat. Commun.*, 2021, **11**, 4004.
2 Y. Pan, S. Fölsch, Y. Nie, D. Waters, Y.-C. Lin, B. Jariwala, K. Zhang, K. Cho, J. A. Robinson and R. M. Feenstra, *Nano Lett.*, 2018, **18**, 1849.
3 E. Li, J.-X. Hu, X. Feng, Z. Zhou, L. An, K. T. Law, N. Wang and N. Lin, *Nat. Commun.*, 2021, **12**, 5601.
4 J. Yang, X. Yi, Z. Zhao, Y. Xie, T. Miao, H. Luo, H. Chen, Bo Liang, W. Zhu, Y. Ye, J.-Y. You, B. Gu, S. Zhang, F. Zhang, F. Yang, Z. Wang, Q. Peng, H. Mao, G. Liu, Z. Xu, H. Chen, H. Yang, G. Su, H. Gao, L. Zhao and X. J. Zhou, *Nat. Commun.*, 2023, **14**, 4089.
5 K. K. Gomez, W. Mar, W. Ko, F. Guinea and H. C. Manoharan, *Nature*, 2012, **483**, 306.
6 R. Drost, T. Ojanen, A. Harju and P. Liljeroth, *Nat. Phys.*, 2017, **13**, 668.
7 M. R. Slot, T. S. Gardenier, P. H. Jacobse, G. C. P. van Miert, S. N. Kempkes, S. J. M. Zevenhuizen, C. M. Smith, D. Vanmaekelbergh and I. Swart, *Nat. Phys.*, 2017, **13**, 672.
8 M. Gibertini, A. Singha, V. Pellegrini, M. Polini and G. Vignale, *Phys. Rev. B:Condens. Matter Mater. Phys.*, 2009, **79**, 241406R.
9 T. H. Harder, O. A. Egorov, C. Krause, J. Beierlein, P. Gagel, M. Emmerling, C. Schneider, U. Peschel, S. Höfling and S. Klembt, *ACS Photonics*, 2021, **8**, 3193.
10 R. A. Vicencio, C. Cantillano, L. Morales-Inostroza, B. Real, C. Mejía-Cortés, S. Weimann, A. Szameit and M. I. Molina, *Phys. Rev. Lett.*, 2015, **114**, 245503.
11 S. Mukherjee, A. Spracklen, D. Choudhury, N. Goldman, P. Öhberg, E. Andersson and R. R. Thomson, *Phys. Rev. Lett.*, 2015, **114**, 245504.
12 Z. Liu, Z.-F. Wang, J.-W. Mei, Y.-S. Wu and F. Liu, *Phys. Rev. Lett.*, 2013, **110**, 106804.
13 S. Wang, W. Wang, L. Z. Tan, X. G. Li, Z. Shi, G. Kuang, P. N. Liu, S. G. Louie and N. Lin, *Phys. Rev. B:Condens. Matter Mater. Phys.*, 2013, **88**, 245430.
14 F. Klappenberger, D. Kühne, W. Krenner, I. Silanes, A. Arnau, F. J. García de Abajo, S. Klyatskaya, M. Ruben and J. V. Barth, *Nano Lett.*, 2009, **9**, 3509.
15 Y. Jing and T. Heine, *J. Am. Chem. Soc.*, 2019, **141**, 743.
16 L. Yan, O. J. Silveira, B. Alldritt, S. Keizilebieke, A. S. Foster and P. Liljeroth, *ACS Nano*, 2021, **15**, 17813.
17 D. Kumar, J. Hellerstedt, B. Field, B. Lowe, Y. Yin, N. V. Medhekar and A. Schiffrin, *Adv. Funct. Mater.*, 2021, **31**, 2106474.
18 M. Telychko, G. Li, P. Mutombo, D. Soler-Polo, X. Peng, J. Su, S. Song, M. J. Koh, M. Edmonds, P. Jelínek, J. Wu and J. Lu, *Sci. Adv.*, 2021, **7**, eabf0269.
19 L. Z. Zhang, Z. F. Wang, B. Huang, B. Cui, Z. Wang, S. X. Du, H.-J. Gao and F. Liu, *Nano Lett.*, 2016, **16**, 2072.
20 L. Hernandez-Lopez, I. Piquero-Zulaica, C. A. Downing, M. Piantek, J. Fujii, D. Serrate, J. E. Ortega, F. Bartolomé and J. Lobo-Checa, *Nanoscale*, 2021, **13**, 5216.
21 B. Yan, B. Stadtmüller, S. Jakobs, J. Seidel, D. Jungkenn, S. Mathias, M. Cinchetti, M. Aeschlimann and C. Felser, *Nat. Commun.*, 2015, **6**, 10167.
22 A. Barragan, S. Lois, A. Sarasola and L. Vitali, *Nanoscale*, 2022, **14**, 17895.
23 A. Barragan, A. Sarasola and L. Vitali, *Angew. Chem., Int. Ed.*, 2020, **59**, 15599–15602.
24 M. Wolf, E. Knoesel and T. Hertel, *Phys. Rev. B:Condens. Matter Mater. Phys.*, 1996, **54**, R5295.
25 J.-Y. Park, U. D. Ham, S.-J. Kahng, Y. Kuk, K. Miyake, K. Hata and H. Shigekawa, *Phys. Rev. B:Condens. Matter Mater. Phys.*, 2000, **62**, R16341.
26 Z. Li, L. Wang, H. Feng, Q. Gao, X. Xu, W. Hao, X. Wang, C. Zhang, K. Wu, S. X. Dou, L. Chen, Z. Hu and Y. Du, *Sci. Adv.*, 2018, **4**, eaau4511.
27 C. Barrateau, F. Ducastelle and T. Mallah, *J. Phys.: Condens. Matter*, 2017, **29**, 465302.

28 T. S. Gardenier, J. J. van den Broeke, J. R. Moes, I. Swart, C. Delerue, M. R. Slot, C. M. Smith and D. Vanmaekelbergh, *ACS Nano*, 2020, **14**, 13638.
29 H. Takeda, T. Takashima and K. Yoshino, *J. Phys.: Condens. Matter*, 2004, **16**, 6317.
30 W.-X. Qiu, S. Li, J.-H. Gao, Y. Zhang and F. C. Zhang, *Phys. Rev. B*, 2016, **94**, 241409R.
31 S. E. Freeney, S. T. P. Borman, J. W. Hartevel and I. Swart, *SciPost Phys.*, 2020, **9**, 085.
32 Y. X. Jiang, J.-X. Yin, M. M. Denner, N. Shumiya, B. R. Ortiz, G. Xu, Z. Guguchia, J. He, M. S. Hossain, X. Liu, J. Ruff, L. Kautzsch, S. S. Zhang, G. Chang, I. Belopolski, Q. Zhang, T. A. Cochran, D. Multer, M. Litskevich, Z.-J. Cheng, X. P. Yang, Z. Wang, R. Thomale, T. Neupert, S. D. Wilson and M. Z. Hasan, *Nat. Mater.*, 2021, **20**, 1353.
33 C. Guo, C. Putzke, S. Konyzheva, X. Huang, M. Gutierrez-Amigo, I. Errea, D. Chen, M. G. Vergniory, C. Felser, M. H. Fischer, T. Neupert and P. J. W. Moll, *Nature*, 2022, **611**, 461.
34 X. G. Juarez, F. Freire-Fernández, S. Khorasani, M. R. Bourgeois, Y. Wang, D. J. Masiello, G. C. Schatz and T. W. Odom, *ACS Photonics*, 2024, **11**, 673.